Theoretical and Applied Mechanics Letters 15 (2025) 100613

Contents lists available at ScienceDirect

Theoretical and Applied Mechanics Letters

journal homepage: www.elsevier.com/locate/taml

Mechanical behaviors of filopodia protrusion-driven cell fusion

Chaohui Jiang [a,b], Zhou Fang [a], Guangsong Xie [a,b], Mei Yang [a,b], Dechang Li [a,*], Baohua Ji [a,c,*]

[a] Institute of Biomechanics and Applications, Department of Engineering Mechanics, Zhejiang University, Hangzhou 310027, China
[b] Wenzhou Institute, University of Chinese Academy of Sciences, Wenzhou 325001, China
[c] Eye Center, The Second Affiliated Hospital of Zhejiang University School of Medicine, Hangzhou 310029, China

ARTICLE INFO

Keywords:
Spontaneous cell fusion
Filopodia interaction
Membrane curvature
Actin polymerization
Syncytia formation
Substrate pattern

ABSTRACT

Cell fusion is a basic biological process that plays critical roles in both physiological and pathological processes. However, how mechanical factors influence the fusion process is not fully understood. In this study, we reported filopodia-mediated fusion among MCF-7 cells. We showed that the filopodia protrusion force induced significant bending of the cell membrane, which was essential for membrane fusion between neighboring cells, and then eventually induced the formation of multinucleated syncytia. The inhibition of actin polymerization significantly reduced the fusion ratio, whereas increased actin polymerization promoted fusion. We found that several factors influence the fusion process, e.g., the cell density, substrate pattern, and stiffness. For example, cell density has a significant effect on cell fusion. There was an optimal cell density for cell fusion. The fusion probability increased with increasing cell density within a moderate cell density range but decreased within a high cell density range. Substrate properties also influence the fusion behavior. For example, the fusion ratio was reduced on nanogrooved surfaces and soft substrates because the surface pattern restricted cell alignment and motility, and soft substrates reduced the activity of the actin dynamics of filopodia for cell fusion. This study not only contributes to our understanding of the basic biology of cell fusion but also has important implications for understanding the mechanisms of cancer progression and potential therapeutic intervention methods.

1. Introduction

Cell fusion is a complex and dynamic biological process that plays critical roles in both physiological and pathological processes [1]. In physiological processes, cell fusion plays important roles in muscle development [2], bone remodeling [3], and placental formation [4], whereas in pathological contexts, it is associated with inflammation [5], cancer progression [6], and the formation of virus-induced syncytia [7]. The formation of multinucleated syncytia may contribute to increased genetic and phenotypic diversity within tumors, enhancing their adaptability and resilience to environmental challenges [8,9]. Furthermore, syncytia can also drive genomic instability and increase metastatic potential [10]. Despite its importance, the mechanisms governing cell fusion, particularly the mechanical mechanisms, remain poorly understood. This knowledge gap is particularly pressing, considering the potential of fusion events to drive tumor evolution and metastasis [11].

In addition to specific fusogenic proteins and signaling pathways [1], spontaneous fusion in cells is thought to rely on intrinsic cellular properties and interactions mediated by the cytoskeleton and cell membranes [12]. However, the precise mechanisms underlying this phenomenon, such as the role of actin cytoskeleton reorganization and the formation of cellular structures such as filopodia, remain largely unexplored. Filopodia [13], which are actin-based cell protrusions, are known to mediate a variety of cellular interactions, including adhesion [12,14], signaling [15], and substance exchange between cells [16,17]. In the context of cell fusion, filopodia act as mediators for initiating physical contact and facilitating the merging of plasma membranes. The dynamic nature of filopodia positions them as potential drivers of syncytium formation. However, their involvement in spontaneous cell fusion has yet to be systematically investigated, and the interplay between filopodia dynamics and cell fusion efficiency remains unclear.

In addition to the cellular structure, the microenvironment of cells [18–20] profoundly influences cell behavior and fate. Factors such as cell density [21], substrate stiffness [22], and surface topography [23] regulate cellular motility, cytoskeletal tension, and the frequency of intercellular interactions. For example, denser cellular arrangements may increase opportunities for physical contact, whereas substrate stiffness may modulate the mechanical properties of cells [24], affecting their ability to initiate and sustain fusion. In addition, membrane curvature and lipid organization at the contact area may play critical roles in modulating fusion efficiency. However, the mechanistic relationship between these physical properties and the fusion process remains largely

* Corresponding authors.
E-mail addresses: dcli@zju.edu.cn (D. Li), bhji@zju.edu.cn (B. Ji).

https://doi.org/10.1016/j.taml.2025.100613
Received 15 April 2025; Received in revised form 20 August 2025; Accepted 21 August 2025
Available online 22 August 2025
2095-0349/© 2025 The Authors. Published by Elsevier Ltd on behalf of The Chinese Society of Theoretical and Applied Mechanics. This is an open access article under the CC BY-NC-ND license (http://creativecommons.org/licenses/by-nc-nd/4.0/)

unexplored. Understanding how these external cues influence fusion behaviors would offer insights into the broader principles of cellular organization and tumor progression.

In this study, we aimed to elucidate the mechanical mechanisms of cell fusion by integrating experimental and molecular dynamics simulation approaches. Specifically, we seek to investigate the role of filopodia in mediating intercellular interactions for fusion, examine how the extracellular environment regulates fusion efficiency, and employ computational models to probe the underlying mechanisms that govern membrane fusion. Our study aims to provide new insights into the mechanisms of spontaneous cell fusion, which could deepen our understanding of its role in tumor biology and therapeutic techniques.

2. Results

2.1. Spontaneous formation of syncytia: membrane fusion dynamics and nuclear redistribution

We observed that a collection of multinucleated syncytia appeared within the MCF-7 cell population during routine cultivation (Fig. 1(a)). Statistical analysis revealed that the syncytia accounted for as much as 10.74% of the MCF-7 cell population (Fig. 1(b)). Further analyses revealed that binucleated syncytia were the most prevalent, comprising 55.3% of the total syncytia (Fig. 1(b)), whereas the proportion of syncytia gradually decreased with increasing number of nuclei. Notably, syncytia with odd numbers of nuclei were less common than those with even numbers of nuclei.

To delve deeper, we captured the complete process of spontaneous cell fusion via time-lapse imaging. Figure 1(c) (I–IV) shows typical stages of the spontaneous cell fusion process in temporal order, demonstrating the gradual disappearance of the boundary between two fused cells. Figure 1(d) displays time-lapse images of the fusion interface at the basal plane of the cells, where the fusion interface propagates and eventually vanishes as the cells fuse into one entity.

Next, we labeled the MCF-7 cell membranes with DiO (green fluorescence) and DiI (magenta fluorescence) to image the membrane fusion dynamics process (Fig. A1(a)). During the fusion process, the fluorescence from the magenta cell diffused into the originally green cell and vice versa, resulting in syncytia with both magenta and green fluorescence. When one cell stably expressed LifeAct-GFP (green cytoplasmic fluorescence) and the other was membrane-stained with DiI (magenta fluorescence), the resulting syncytia exhibited green cytoplasmic fluorescence and magenta membrane fluorescence (Fig. 1(e)). Interestingly, the cytoplasmic fluorescence homogenized rapidly (in 20 min), whereas the membrane fluorescence transferred more slowly (in 60 min) between the two cells (Fig. 1(e)).

To confirm that the syncytia originated from different cells rather than from abnormal division of a single cell, we fused the cells co-transfected with LifeAct and H2B (green cytoplasm, orange nuclei) with Hoechst-and DiD-stained cells (blue nuclei, magenta membrane). The resulting syncytia contained green cytoplasmic fluorescence, magenta membrane fluorescence, and two distinct nuclei: one orange (H2B-labeled) and one blue (Hoechst-stained) (Fig. 1(f)). Furthermore, we observed that the nuclei initially lacking H2B fluorescence gradually obtained fluorescence after fusion (Fig. 1(g)), indicating that the diffusion of H2B protein and dynamic chromatin reorganization within the shared cytoplasm played important roles. H2B, a histone protein, plays a key role in chromatin structure and function, and its redistribution suggests that chromatin remodeling occurs in fused nuclei.

2.2. The role of filopodia and actin dynamics in spontaneous cell fusion

To explore further details of spontaneous fusion, we used short-interval time-lapse imaging and slice-based 3D reconstruction to capture the dynamic process of spontaneous fusion. We found that there was prolonged interaction between the filopodia of two neighboring cells prior to fusion (Fig. 2(a)–(b), Videos 1–2). These interactions persisted until the cell boundaries began to break, underscoring the crucial role of filopodia in the fusion process. We categorized the fusion events into two types: fusion between cells separated by a certain distance, as shown in Fig. 2(a), and fusion between contacting cells, as captured in Fig. 2(b). Our findings indicated that the time for cell fusion is longer for cells in close proximity than for those separated by a certain distance (Fig. 2(c)).

To validate the role of filopodia and actin dynamics in cell fusion, we treated the cells with inhibitors and promoters. Our results revealed that CytoD (which inhibits actin polymerization), ML141 (which blocks Cdc42 to suppress filopodia formation), and NSC23766 (which inhibits Rac1 to prevent lamellipodia formation) significantly reduced the fusion probability (Fig. 2(d) and Fig. A1(b)). Notably, suppressing lamellipodia had a smaller effect than disrupting actin polymerization or filopodia formation. Conversely, jasplakinolide (which promotes actin polymerization and stabilizes actin filaments) increased the fusion ratio (Fig. 2(e) and Fig. A1(c)), highlighting the importance of actin dynamics and filopodia protrusion in cell fusion. Additionally, disrupting cell-cell adhesion with EDTA still allowed initially unconnected cells to fuse through extended filopodia (Fig. A1(d)). The fusion ratio of EDTA-treated cells was not significantly different from that of control cells, suggesting that cell–cell adhesion may not be essential for fusion (Fig. 2(f)).

2.3. Effects of cell density, substrate surface structure, and substrate stiffness on spontaneous cell fusion

Next, we examined how the cell density and substrate properties affect cell fusion. The cell density has a significant effect. For low-density cells (<350 cells·mm^{-2}), the space between cells is large, making it difficult for cells to come into contact (Fig. 3(a)). The fusion probability increased as the density increased from (<350 cells· mm^{-2}) to 350–700 cells·mm^{-2}. The fusion efficiency was highest within this intermediate range (350–700 cells·mm^{-2}), indicating that this range represents the optimal cell density for fusion. However, at very high cell densities, the fusion probability decreased when the cell density further increased (Fig. 3(b)). There might be two mechanisms underlying the cell density effect at such high densities. One is that the cell density influences active motility, allowing cells to find a proper orientation/contact for cell fusion. The second factor is that it influences the necessary protrusion length of the filopodia necessary for the fusion process.

To assess the impact of the substrate surface structure, we cultured the cells on the nanogrooved surfaces, on which the cells aligned along the direction of the grooved pattern (Fig. 3(c)). The fusion ratios significantly decreased on these surfaces (Fig. 3(d)), as the surface structure constrained cell motility, which then reduced the likelihood of proper contact between neighboring cells for fusion (Fig. 3(e)).

Finally, we investigated the effect of substrate stiffness on syncytia formation. The cells spread more extensively on the stiffer substrates (Fig. 3(f)), and the proportion of syncytia formed was consistently greater on the stiffer substrates at both 24 and 48 h (Fig. 3(g)). These findings suggest that stiffer substrates promote syncytia formation, possibly by enhancing cytoskeletal organization, particularly filopodia protrusion, facilitating the mechanical interactions required for cell fusion.

2.4. Filopodia-mediated membrane fusion under varying intercellular distances

Our experiments demonstrated that filopodia interactions between neighboring cells are critical for cell fusion; however, excessive cell density paradoxically reduces the fusion ratio (Fig. 3(b)). We propose that this strange phenomenon is due to the reduced membrane curvature at filopodia-mediated contact sites between cells at very high cell density. To validate this hypothesis, we conducted a systematic molecular dynamic simulation across a spectrum of intercellular distances, with

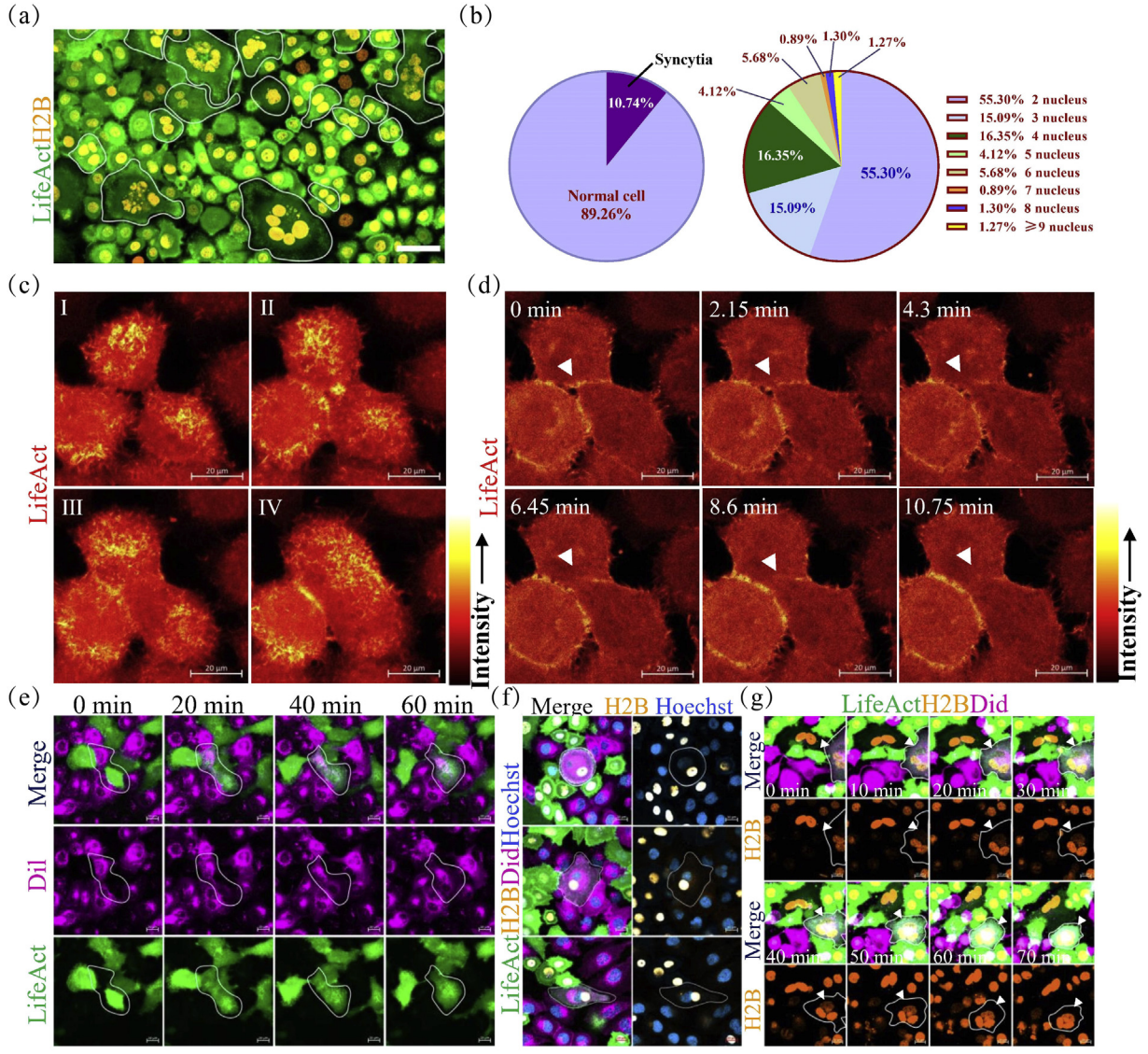

Fig. 1. Spontaneous formation of syncytia: membrane dynamics and nuclear redistribution.
(a) Fluorescence imaging of the MCF-7 cell line cultured on a confocal dish. The green fluorescence represents LifeAct, whereas the orange fluorescence represents H2B. The scale bar represents 50 μm.
(b) Proportion of multinucleated syncytial cells to mononucleated cells (left). Proportion of multinucleated cells with different numbers of nuclei within the syncytium (right).
(c) I–IV: Key frames of the spontaneous cell fusion process in temporal order. Red fluorescence represents LifeAct. The scale bar represents 20 μm.
(d) Time series of the extended fusion interface between two cells at the bottom of the cell, with white arrows indicating the sites of cell contact and fusion. The fusion interfaces gradually extend. Red fluorescence represents LifeAct. The scale bar represents 20 μm.
(e) Cytoplasmic (green) mixing occurs rapidly (in 20 min) during cell fusion, whereas membrane (magenta) fusion into the syncytium takes more time (in 60 min). The top row shows the merged image, the middle row displays the magenta fluorescence of the cell membrane stained with DiI, and the bottom row shows the green fluorescence of the cytoskeleton labeled with LifeAct. The scale bar represents 20 μm.
(f) The fusion of cells into a syncytium results in green fluorescence in the cytoplasm and magenta fluorescence in the cell membrane. One of the nuclei emits orange fluorescence from H2B, while the other nucleus emits blue fluorescence from Hoechst. The first column shows the merged image, whereas the second column displays the merged image of the two nuclear channels, with different-colored nuclei representing different origins. The scale bar represents 20 μm.
(g) Following cell fusion, the initially nonfluorescent nucleus gradually acquires orange fluorescence from H2B. The first and third rows show the merged image, whereas the second and fourth rows display the orange single-channel image of the H2B-transfected nucleus. Green fluorescence represents LifeAct, magenta represents the cell membrane, and orange represents H2B. The scale bar represents 20 μm.

particular emphasis on the effects of membrane curvature on filopodia interactions.

To analyze the effect of membrane curvature on the fusion process, we established a coarse-grained modeling system including two actin filaments and two 100 nm × 100 nm POPC lipid bilayers, mimicking the contact zone between two neighboring cells about to fuse (Fig. A2). A modified Dry-MARTINI force field was adopted in the molecular dynamic simulations considering the balance between computational efficiency and structural fidelity. The detailed force field parameterization and simulation protocols are systematically documented in the Methods section. The phospholipid bilayer membranes protrude from the vertically aligned actin filaments at a given distance between the two membranes (Fig. A2). Under quasistatic loading by the actin filaments, the two membranes began to establish contact, as illustrated and defined in

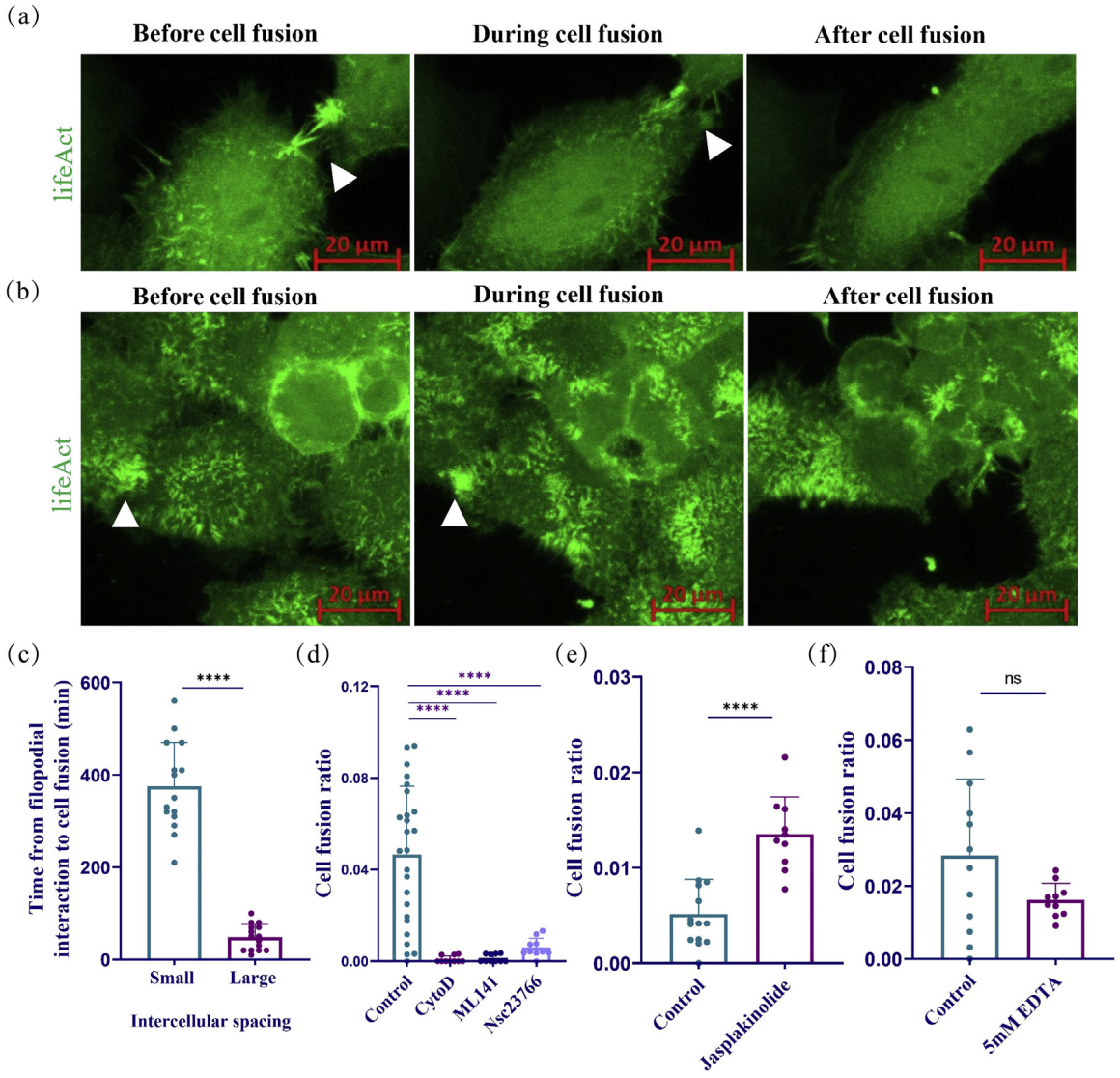

Fig. 2. The role of filopodia protrusion and actin dynamics in spontaneous cell fusion.
(a) Illustrating the stages of cell fusion: before, during, and after fusion, with the two cells initially separated by a certain distance. Prior to fusion, the two cells interacted through the extension of filopodia. Green fluorescence represents LifeAct. The scale bar represents 20 μm.
(b) Illustrating the stages of cell fusion: before, during, and after fusion, with the two cells closely apposed. Prior to fusion, the two cells interact through the extension of filopodia. Green fluorescence represents LifeAct. The scale bar represents 20 μm.
(c) The time from filopodial interaction to complete cell fusion was longer for cells in close proximity than for those separated by a certain distance. Error bar: mean ± SD; unpaired *t*-test, $^{****}p < 0.0001$, $n = 15$.
(d) Treatment with CytoD, ML141, or NSC23766 significantly reduced the cell fusion ratio in MCF-7 cells. Error bar: mean ± SD; one-way ANOVA, $^{****}p < 0.0001$, $n = 25$ for the control, $n = 10$ for cytoD/ML141/nsc23766.
(e) Jasplakinolide treatment increases the cell fusion ratio in MCF-7 cells. Error bar: mean ± SD; unpaired *t*-test, $^{****}p < 0.0001$, $n = 14$ for the control, $n = 10$ for jasplakinolide.
(f) EDTA treatment has no significant effect on the cell fusion ratio in MCF-7 cells. Error bar: mean ± SD; unpaired *t*-test, p(not significant)=0.0899, $n = 12$ for the control, $n = 10$ for 5 mM EDTA.

Supplementary Fig. A3. Four different membrane distances (dz) = 25, 35, 45 and 55 nm were adopted in the simulations (Fig. 4(a)), representing typical filopodia contact states under varying intercellular distances.

The time intervals from the initial contact of the hydrophilic head groups to the subsequent hydrophobic tail group interactions between the two membranes were calculated for four different intermembrane spacings, as shown by the histogram in Fig. 4(b). We can see that there is an inverse correlation between dz and the fusion time, which aligns with the experimental observations that the fusion efficiency decreased when the cell density was increased to a high level (Fig. 2(c)).

Figure 4(c) shows the molecular details of the fusion process at the contact area of the two membranes. Following the hydrophilic head group contact, transient hydrophobic defects were exposed at high-curvature domains of the bent membrane under the protrusion force of actin filaments. Subsequent thermal fluctuation-driven collisions between the exposed hydrophobic tail groups initiated the membrane fusion process, with complete lipid mixing occurring within approximately 3000 ps.

Figure 4(d) shows the defect distribution on the bent membrane surfaces for different intermembrane distances. Our results revealed a positive correlation between the interbilayer distance and the membrane

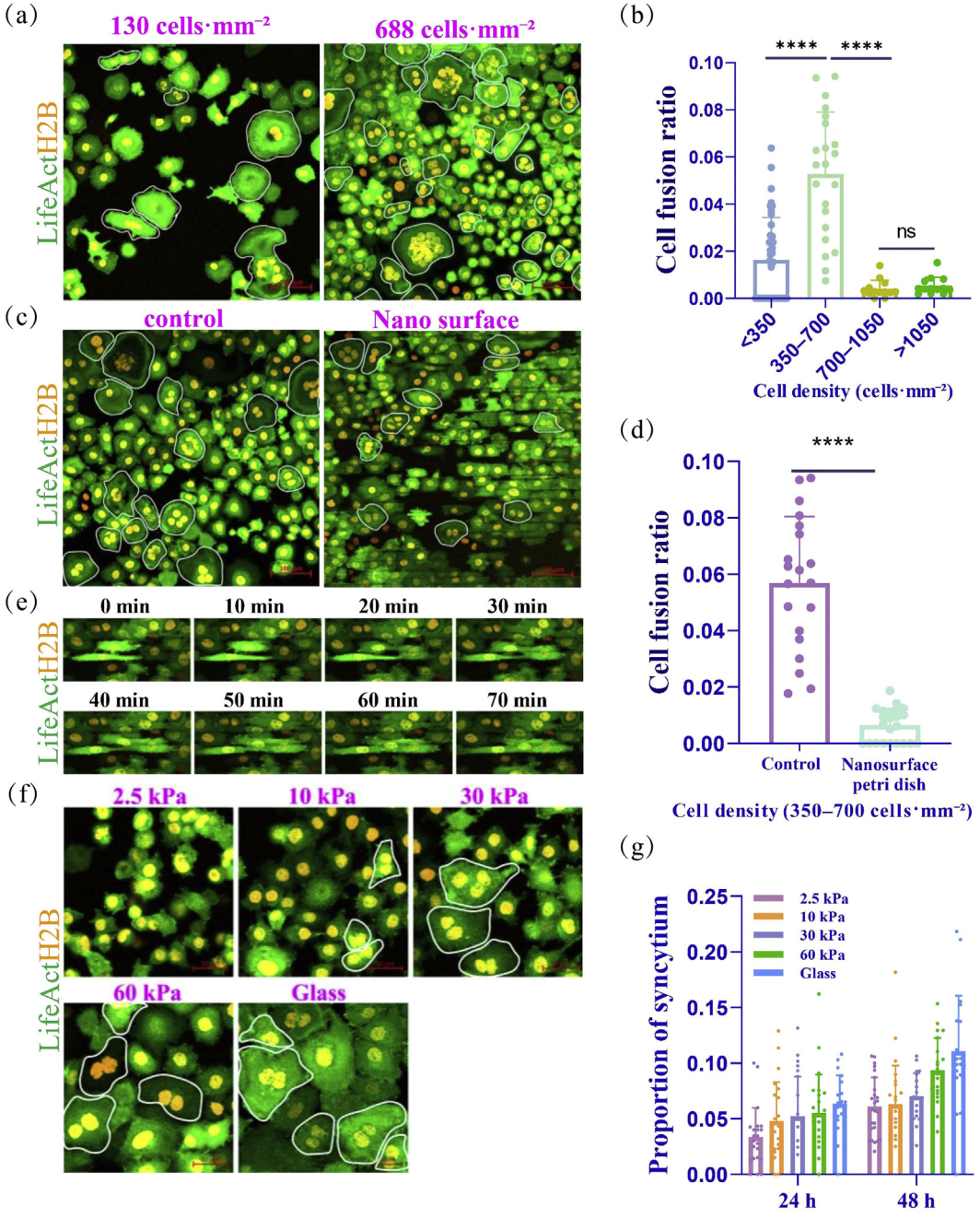

Fig. 3. Effects of environmental factors on spontaneous cell fusion: cell density, substrate surface structure, and substrate stiffness.
(a) Fluorescence images of the fused cells at different cell densities. Green fluorescence represents LifeAct, and orange represents H2B. The scale bar represents 100 μm.
(b) Effect of cell density on the cell fusion ratio. Error bar: mean ± SD; one-way ANOVA, $^{****}p < 0.0001$, p(not significant) = 0.9981, n = 40 for < 350, n = 22 for 350–700, n = 13 for 700–1050, n = 13 for >1050.
(c) Fluorescence images of MCF-7 cells cultured on a glass-bottom confocal dish and a nanostructured surface Petri dish. Green fluorescence represents LifeAct, and orange fluorescence represents H2B. The scale bar represents 100 μm.
(d) The cell fusion ratio was significantly reduced in MCF-7 cells cultured on a nanosurface Petri dish. Error bar: mean ± SD; unpaired t-test, $^{****}p < 0.0001$, n = 20 for the control, n = 23 for the nanostructured surface Petri dish.
(e) Time series of spontaneous cell fusion in MCF-7 cells cultured on a nanosurface Petri dish. Green fluorescence represents LifeAct, and orange fluorescence represents H2B. The scale bar represents 20 μm.
(f) Fluorescence images of MCF-7 cells cultured on substrates with varying stiffnesses (2.5 kPa, 10 kPa, 30 kPa, and 60 kPa) and on a glass substrate. Green fluorescence represents LifeAct, and orange fluorescence represents H2B. The scale bar represents 50 μm.
(g) Increased syncytium formation on stiffer substrates (2.5 kPa, 10 kPa, 30 kPa, and 60 kPa) at both 24 and 48 h in MCF-7 cells. Error bars: mean ± SD; n = 20–25.

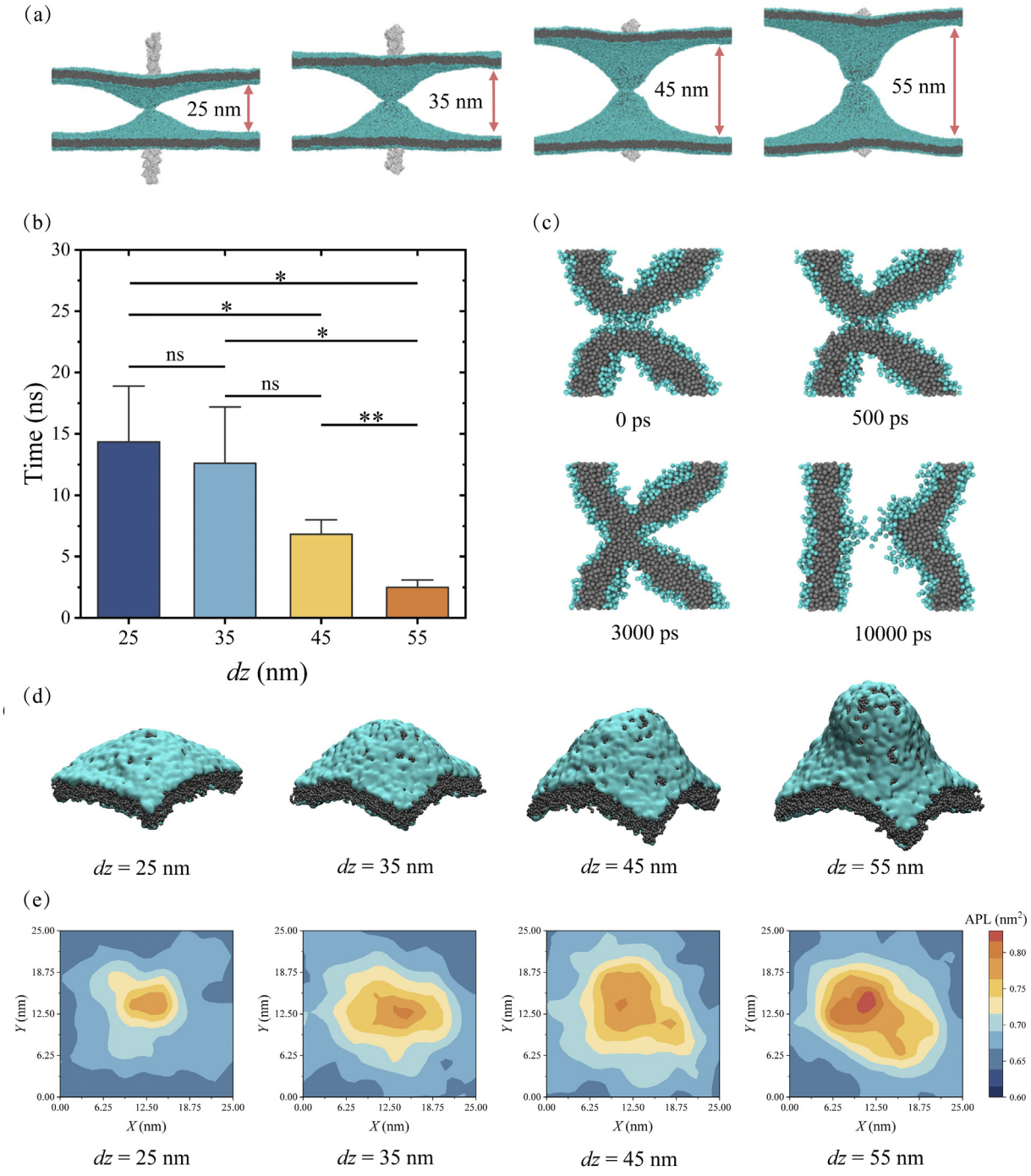

Fig. 4. Filopodia-mediated membrane fusion under varying intercellular distances.
(a) Coarse-grained membrane contact models with intermembrane distances of 25, 35, 45, and 55 nm. Molecular representations: white (coarse-grained actin filaments), blue (POPC hydrophilic head groups), gray (hydrophobic lipid tails).
(b) Histogram of time intervals from membrane contact to complete fusion across different spacings. Error bars: mean ± SD; $^{*}p < 0.05$, $^{**}p < 0.01$, ns indicates no significant difference; $n = 3$.
(c) Sequential snapshots illustrating the contact–to–fusion transition of two neighboring membranes.
(d) Defect distribution maps within the contact regions at different intermembrane distances.
(e) Per-lipid area distributions in the contact regions at different intermembrane distances.

defect density, suggesting greater expansion of the area per lipid (APL) at greater dz (Fig. 4(e)), which thermodynamically favors the exposure of hydrophobic tails. The spatial congruence between regions with high APLs and regions with high curvatures further confirmed this mechanism, as shown in Supplementary Fig. A4. This APL-curvature codependency provides molecular validation of our hypothesis that the reduced membrane curvature at high cell densities impairs the membrane fusion process.

3. Discussion

This study performed a combined experimental and modeling investigation to understand the mechanisms driving cell fusion in MCF-7 cells. Cell fusion can introduce genomic instability and facilitate metastatic potential [10], and cytoplasmic mixing during fusion should also promote intercellular exchange of key signaling molecules, which may further promote tumor progression [25]. The molecular mechanical mechanisms of the actin-driven fusion process were analyzed via molecular dynamics simulations, which offer deeper insight into how membrane curvature modulates fusion efficiency. The chemical/structural and mechanical factors, including filopodia actin dynamics, cell density, substrate surface pattern and stiffness, that influence fusion efficiency were analyzed.

Our experiments revealed the pivotal roles of filopodia in mediating cell fusion. High-resolution imaging revealed that prolonged filopodia interactions were essential precursors for intercellular membrane fusion, establishing physical connections/contacts between cells. The inhibition of actin polymerization or filopodia formation substantially reduced the fusion ratios. In contrast, increased actin polymerization accelerated fusion, highlighting the role of actin dynamics as a key driving force of cell fusion. Interestingly, disrupting intercellular adhesion did not hinder fusion, suggesting that intercellular adhesion is not necessary for this filopodia-driven cell fusion. These results revealed a new mechanical function of actin dynamics in driving the cell fusion process.

In addition to the role of actin dynamics, our results highlighted the influence of the extracellular environment on fusion events. First, the cell density has a biphasic effect on the fusion ratio, suggesting an optimal cell density at which the fusion efficiency peaks owing to the balance between the probability of intercellular contact and the degree of extension of filopodia for fusion. For example, at very low cell density, neighboring cells had a smaller probability of contact for fusion. In contrast, at very high density, a relatively small intercellular space restricts filopodia extension, reducing the number of fusion events. Moreover, the fusion ratio was also reduced on nanogrooved surfaces because the directional alignment of cells restricted the motility of the cells and thus the probability of contact, thereby reducing the likelihood of cell fusion. These findings emphasized the roles of cellular filopodia extension and freedom of interaction in cell fusion. Third, substrate stiffness is also a key environmental factor. The increased formation of syncytia on stiffer substrates suggests a direct link between stiffness and fusion probability. Stiffer substrates likely increase cytoskeletal tension and organization, facilitating the mechanical interactions necessary for fusion.

While this study focused on the individual effects of cell density, substrate surface topography and stiffness on fusion efficiency, these factors rarely act independently; instead, they act together. Multiple environmental cues likely coordinate cell fusion synergistically by influencing intercellular contact, alignment, and local mechanical forces at cell interfaces. Specifically, substrate stiffness significantly affects cell spreading [26], which alters cell density and intercellular interactions. When the substrate stiffness is sufficiently high, the cell behavior is governed mainly by the topographical features of the substrate. However, when the substrate is soft, the topography and stiffness interact, corporately shaping the perceived mechanical environment of the cells [27]. This synergy may optimize cell spreading, promote specific cell alignments, and provide coordinated mechanical signals, driving membrane remodeling and cell fusion. Although this study did not systematically validate these multifactor interactions, the findings suggested that cell fusion was regulated by a complex network of biophysical signals. Future research should incorporate these interactions into multiparameter experimental designs and advanced models to gain a deeper understanding of the biophysics behind cell fusion.

To address the underlying mechanisms of the effect of high cell density, we conducted molecular dynamics simulations to simulate the cell fusion facilitated by filopodial protrusions. We found that the curvature of the deformed membrane under the protrusion force of filopodia had a significant effect on fusion. When the cell density increased, the protrusion length of the filopodia decreased as the distance between two neighboring cells decreased, and the curvature of the two contacting neighboring cell membranes under the protrusion force also decreased. Our simulations revealed that the smaller the curvature of the cell membrane was, the fewer hydrophobic defects there were on the membrane, which was not favorable for the fusion process; thus, the fusion ratio was reduced. In contrast, a greater intermembrane distance was associated with greater curvature of the protruded membrane, which favored the formation of membrane defects for fusion. In addition, increased cell density would also apply spatial constriction between/among neighboring cells, which would reduce the active motion for optimal contact for fusion.

In conclusion, this study provides an integrated experimental and theoretical framework for understanding the mechanisms driving spontaneous cell fusion in MCF-7 cells. Several factors influence the fusion process, e.g., the cell density, substrate surface pattern and stiffness. Moreover, molecular dynamics simulations offer deeper insight into how membrane curvature modulates fusion efficiency, establishing a new dimension for our understanding of fusion regulation. These findings pave the way for future research to explore the molecular pathways governing fusion dynamics, their functional consequences in cancer, and potential therapeutic strategies to target fusion-related processes in tumor progression.

4. Materials and methods

4.1. Lentiviral transduction

HEK293T cells were seeded in a 100 mm culture dish and grown to approximately 80% confluence. The cells were then transfected with 5 μg of LifeAct-ZsGreen plasmid and 5 μg of packaging vectors (psPAX2 and pMD2.G). Lentiviral supernatants were collected twice daily over two consecutive days, filtered through a 0.22 μm syringe filter, and stored at −80 °C. For infection, the viral supernatant was supplemented with 10 $\mu g \cdot mL^{-1}$ polybrene and used to infect MCF-7 cells. Successfully infected cells were selected via fluorescence-activated cell sorting (FACS). After generating LifeAct-ZsGreen-transfected MCF-7 cells, the LifeAct-ZsGreen plasmid was replaced with the H2B-mCherry plasmid, and the transduction process was repeated to obtain MCF-7 cells coexpressing LifeAct (green) and H2B (orange).

4.2. Cell culture and treatments

MCF-7 cells (human breast cancer cells), including LifeAct-transfected, LifeAct and H2B-cotransfected, and nontransfected MCF-7 cells, were cultured in a humidified incubator at 37 °C with 5% CO_2 in DMEM (Sigma) supplemented with 10% fetal bovine serum (FBS, Gibco) and 1% penicillin–streptomycin (P/S, Gibco). Subculturing was performed using 0.25% trypsin–EDTA (Gibco) for cell dissociation.

To inhibit actin polymerization, cytochalasin D (MedChemExpress) was applied at a concentration of 2 μM. ML141 (Beyotime) was used at 10 μM to block Cdc42 GTPase, thereby suppressing filopodia formation. NSC23766 (MedChemExpress) at 10 μM was used to inhibit Rac1 activation, preventing lamellipodia formation. Jasplakinolide (MedChemExpress), at a concentration of 1 μM, was applied to promote actin poly-

merization and stabilize actin filaments. EDTA (Macklin) at 5 mM was used to disrupt the intercellular junctions.

To exclude syncytia from the cell population, we used a 20 μm cell strainer (greiner) to separate larger multinucleated cells from single cells. To constrain the cells into a unidirectional alignment, we used 35 mm NanoSurface Dishes (NanoSurface Biomedical), which feature parallel nanogrooves on the culture surface. These grooves are engineered to guide cell alignment through contact guidance and have a pitch of 0.8 μm, a groove width of 0.8 μm, and a depth of 0.6 μm.

4.3. Membrane and nuclear staining

For membrane staining, DiO, DiI, and DiD (Beyotime, 1 μM) were used. The dyes were mixed with the culture medium, and the cells were incubated for 1 hour. After staining, the cells were dissociated, centrifuged to remove excess dye, and seeded into confocal dishes. The cells were allowed to spread for 10 h before time-lapse imaging of cell fusion was conducted. Additionally, 1 $\mu g \cdot mL^{-1}$ Hoechst (Thermo Fisher) was used for nuclear staining.

4.4. Preparation of gel substrates

Polyacrylamide substrates were prepared following established protocols with minor modifications [28]. To create 2.5, 10, 30, and 60 kPa polyacrylamide substrates, we used a constant acrylamide concentration of 10% ($w \cdot v^{-1}$) and adjusted the bis-acrylamide concentration to 0.03%, 0.05%, 0.17%, and 0.35% ($w \cdot v^{-1}$), respectively. First, glass slides were pretreated with repel-silane (Sigma), and round coverslips were treated with bind-silane (Sigma). Acrylamide and N,N-methylene-bis-acrylamide (Bio-Rad) were mixed with fluorescent beads (Sigma) and a curing agent. This mixture was then sandwiched between a pretreated glass slide and a coverslip to form a flat gel layer approximately 100 μm thick. After the polyacrylamide gel solidified, the glass slide was peeled off, leaving the gel to adhere to the coverslip. The gel surface was washed with HEPES, coated with sulfo-SANPAH (Thermo Fisher, Pierce), and sterilized by UV irradiation for 30 min. A 300 μL droplet of collagen type I (Corning, 0.2 mg mL^{-1}) solution was then applied to the surface of the gel and incubated overnight at 4 °C. Following incubation, the gel substrate was sterilized again under UV light. After sterilization, the polyacrylamide substrate was immersed in culture medium and incubated as required for the experiment.

4.5. Simulation setup and parameters

Filopodial contact at the tapered tip is a prerequisite for initiating cell fusion. Confocal microscopy illustrated the progressive filopodium tapering toward distal ends (Fig. A5(a)), whereas electron microscopy data from Sorrentino et al. [29] demonstrated that these terminal structures comprise single actin filaments enveloped by phospholipid membranes. Guided by these ultrastructural insights, we constructed a filopodia contact model (Fig. A5(b)) for molecular dynamics simulations, replicating the membrane-encapsulated actin protrusion architecture observed at filopodial tips.

In the simulations, we employed a modified Dry Martini force field [30] wherein protein–protein interactions were intentionally excluded owing to known inaccuracies in protein parameterization within the standard Dry Martini framework. Specifically, all protein–protein interactions were disregarded in the simulations, whereas the native protein–lipid and lipid–lipid interactions were retained. To better restrict protein conformational changes while specifically emphasizing membrane dynamics, actin filaments were confined under elastic network restraint. All the simulations were conducted via GROMACS [31,32] under NPT ensemble conditions (310 K, 1 bar) with periodic boundary conditions. Electrostatic interactions were calculated via the reaction-field method [33], whereas both Coulomb and van der Waals interactions utilized a 1.2 nm cutoff. The temperature and pressure were regulated through v-rescale [34] and C-rescale [35] algorithms, respectively.

The model consists of two 100 nm × 100 nm POPC coarse-grained POPC lipid bilayers (represented by blue and gray beads) and two coarse-grained actin filaments (white beads), as shown in Fig. A5(b) and (c). In the initial configuration, the two actin filaments were positioned on the opposing surfaces of the two parallel POPC bilayers and aligned, as shown in Fig. A5(c) and (d).

4.6. Data analysis

The experimental images were exported and processed via ImageJ and ZEN BLUE 3.1. Statistical analysis and graphing were performed with GraphPad Prism 8. The cell fusion ratio was quantified as the proportion of fusion events within 10 h relative to the initial cell population. Differences between groups were evaluated via one-way analysis of variance (ANOVA) and t tests. Statistical significance is indicated as follows: $^{*}p < 0.05$, $^{**}p < 0.01$, $^{***}p < 0.001$, $^{****}p < 0.0001$; ns indicates no significant difference. Unless otherwise stated, representative data from at least three independent experiments are shown.

Declaration of competing interest

The authors declare that they have no known competing financial interests or personal relationships that could have appeared to influence the work reported in this paper.

CRediT authorship contribution statement

Chaohui Jiang: Writing – original draft, Methodology, Investigation. **Zhou Fang:** Writing – original draft, Methodology, Investigation. **Guangsong Xie:** Methodology, Investigation. **Mei Yang:** Methodology, Investigation. **Dechang Li:** Writing – original draft, Project administration, Methodology, Investigation. **Baohua Ji:** Writing – original draft, Supervision, Methodology, Investigation, Funding acquisition, Conceptualization.

Acknowledgments

This work was supported by the National Natural Science Foundation of China (Grant Nos. 11932017 and 12122212).

Supplementary materials

Supplementary material associated with this article can be found, in the online version, at doi:10.1016/j.taml.2025.100613.

References

[1] H. Zhang, H. Ma, X. Yang, L. Fan, S. Tian, R. Niu, M. Yan, M. Zheng, S. Zhang, Cell fusion-related proteins and signaling pathways, and their roles in the development and progression of cancer, Front. Cell Dev. Biol. 9 (2022) 809668.
[2] M.J. Petrany, D.P. Millay, Cell fusion: merging membranes and making muscle, Trends Cell Biol. 29 (2019) 964–973.
[3] K. Archacka, I. Grabowska, B. Mierzejewski, J. Graffstein, A. Górzyńska, M. Krawczyk, A.M. Różycka, I. Kalaszczyńska, G. Muras, W. Stremińska, K. Jańczyk-Ilach, P. Walczak, M. Janowski, M.A. Ciemerych, E. Brzoska, Hypoxia preconditioned bone marrow-derived mesenchymal stromal/stem cells enhance myoblast fusion and skeletal muscle regeneration, Stem Cell Res. Ther. 12 (2021) 448.
[4] R.M. Roberts, T. Ezashi, L.C. Schulz, J. Sugimoto, D.J. Schust, T. Khan, J. Zhou, Syncytins expressed in human placental trophoblast, Placenta 113 (2021) 8–14.
[5] I. Singec, E.Y. Snyder, Inflammation as a matchmaker: revisiting cell fusion, Nat. Cell Biol. 10 (2008) 503–505.
[6] D. Duelli, Y. Lazebnik, Cell fusion: a hidden enemy? Cancer Cell 3 (2003) 445–448.
[7] L. Lin, Q. Li, Y. Wang, Y. Shi, Syncytia formation during SARS-CoV-2 lung infection: a disastrous unity to eliminate lymphocytes, Cell Death Different. 28 (2021) 2019–2021.
[8] D. Miroshnychenko, E. Baratchart, M.C. Ferrall-Fairbanks, R.V. Velde, M.A. Laurie, M.M. Bui, A.C. Tan, P.M. Altrock, D. Basanta, A. Marusyk, Spontaneous cell fusions as a mechanism of parasexual recombination in tumor cell populations, Nat. Ecol. Evol. 5 (2021) 379–391.

[9] C.E. Gast, A.D. Silk, L. Zarour, L. Riegler, J.G. Burkhart, K.T. Gustafson, M.S. Parappilly, M. Roh-Johnson, J.R. Goodman, B. Olson, M. Schmidt, J.R. Swain, P.S. Davies, V. Shasthri, S. Iizuka, P. Flynn, S. Watson, J. Korkola, S.A. Courtneidge, J.M. Fischer, J. Jaboin, K.G. Billingsley, C.D. Lopez, J. Burchard, J. Gray, L.M. Coussens, B.C. Sheppard, M.H. Wong, Cell fusion potentiates tumor heterogeneity and reveals circulating hybrid cells that correlate with stage and survival, Sci. Adv. 4 (2018) eaat7828.
[10] L. Delespaul, C. Gélabert, T. Lesluyes, S. Le Guellec, G. Pérot, L. Leroy, J. Baud, C. Merle, L. Lartigue, F. Chibon, Cell–cell fusion of mesenchymal cells with distinct differentiations triggers genomic and transcriptomic remodeling toward tumor aggressiveness, Sci. Rep. 10 (2020) 21634.
[11] M.S. Tretyakova, A.R. Subbalakshmi, M.E. Menyailo, M.K. Jolly, E.V. Denisov, Tumor hybrid cells: nature and biological significance, Front. Cell Dev. Biol. 10 (2022) 814714.
[12] K. Shilagardi, S. Li, F. Luo, F. Marikar, R. Duan, P. Jin, J.H. Kim, K. Murnen, E.H. Chen, Actin-propelled invasive membrane protrusions promote fusogenic protein engagement during cell–cell fusion, Science 340 (2013) 359–363.
[13] P.K. Mattila, P. Lappalainen, Filopodia: molecular architecture and cellular functions, Nat. Rev. Mol. Cell Biol. 9 (2008) 446–454.
[14] F.Pröls Sagar, C. Wiegreffe, M. Scaal, Communication between distant epithelial cells by filopodia-like protrusions during embryonic development, Development 142 (2015) 665–671.
[15] F. Pröls, M.Scaal Sagar, Signaling filopodia in vertebrate embryonic development, Cell. Mol. Life Sci. 73 (2016) 961–974.
[16] C.A. Heckman, H.K. Plummer, Filopodia as sensors, Cell. Sign. 25 (2013) 2298–2311.
[17] J.L. Gallop, Filopodia and their links with membrane traffic and cell adhesion, Semin. Cell Dev. Biol. 102 (2020) 81–89.
[18] E. Jiang, T. Yan, Z. Xu, Z. Shang, Tumor microenvironment and cell fusion, BioMed Res. Int. 2019 (2019) 5013592.
[19] P.V. Shultes, D.T. Weaver, D.S. Tadele, R.J. Barker-Clarke, J.G. Scott, Cell–cell fusion in cancer: the next cancer hallmark? Int. J. Biochem. Cell Biol. 175 (2024) 106649.
[20] T. Dittmar, R. Hass, Extracellular events involved in cancer cell–Cell fusion, Int. J. Mol. Sci. 23 (2022) 16071.
[21] A.J. Loza, S. Koride, G.V. Schimizzi, B. Li, S.X. Sun, G.D. Longmore, Cell density and actomyosin contractility control the organization of migrating collectives within an epithelium, Mol. Biol. Cell 27 (2016) 3459–3470.
[22] P.A. Janmey, D.A. Fletcher, C.A. Reinhart-King, Stiffness sensing by cells, Physiol. Rev. 100 (2020) 695–724.
[23] M.-H. Kim, Y. Sawada, M. Taya, M. Kino-oka, Influence of surface topography on the human epithelial cell response to micropatterned substrates with convex and concave architectures, J. Biol. Eng. 8 (2014) 13.
[24] Y. Zhuang, Y. Huang, Z. He, T. Liu, X. Yu, S.X. Xin, Effect of substrate stiffness on the mechanical properties of cervical cancer cells, Arch. Biochem. Biophys. 725 (2022) 109281.
[25] H.-F. Wang, W. Xiang, B.-Z. Xue, Y.-H. Wang, D.-Y. Yi, X.-B. Jiang, H.-Y. Zhao, P. Fu, Cell fusion in cancer hallmarks: current research status and future indications (Review), Oncol. Lett. 22 (2021) 530.
[26] D.E. Discher, P. Janmey, Y.-l. Wang, Tissue cells feel and respond to the stiffness of their substrate, Science 310 (2005) 1139–1143.
[27] Y. Yang, K. Wang, X. Gu, K.W. Leong, Biophysical regulation of cell behavior—Cross talk between substrate stiffness and nanotopography, Engineering 3 (2017) 36–54.
[28] M. Dembo, Y.-L. Wang, Stresses at the cell-to-substrate interface during locomotion of fibroblasts, Biophys. J. 76 (1999) 2307–2316.
[29] S. Sorrentino, J.J. Conesa, A. Cuervo, R. Melero, B. Martins, E. Fernandez-Gimenez, F.P. de Isidro-Gomez, J. de la Morena, J.-D. Studt, C.O.S. Sorzano, M. Eibauer, J.M. Carazo, O. Medalia, Structural analysis of receptors and actin polarity in platelet protrusions, Proc. Natl. Acad. Sci. 118 (2021) e2105004118.
[30] C. Arnarez, J.J. Uusitalo, M.F. Masman, H.I. Ingólfsson, D.H. de Jong, M.N. Melo, X. Periole, A.H. de Vries, S.J. Marrink, Dry Martini, a coarse-grained force field for lipid membrane simulations with implicit solvent, J. Chem. Theory Comput. 11 (2015) 260–275.
[31] D. Van Der Spoel, E. Lindahl, B. Hess, G. Groenhof, A.E. Mark, H.J.C. Berendsen, GROMACS: fast, flexible, and free, J. Comput. Chem. 26 (2005) 1701–1718.
[32] M.J. Abraham, T. Murtola, R. Schulz, S. Páll, J.C. Smith, B. Hess, E. Lindahl, GROMACS: high performance molecular simulations through multilevel parallelism from laptops to supercomputers, SoftwareX. 1-2 (2015) 19–25.
[33] I.G. Tironi, R. Sperb, P.E. Smith, W.F. van Gunsteren, A generalized reaction field method for molecular dynamics simulations, J. Chem. Phys. 102 (1995) 5451–5459.
[34] G. Bussi, D. Donadio, M. Parrinello, Canonical sampling through velocity rescaling, J. Chem. Phys. 126 (2007) 014101.
[35] M. Bernetti, G. Bussi, Pressure control using stochastic cell rescaling, J. Chem. Phys. 153 (2020) 114107.